VIP *Very Important Paper*

Special Collection

Small Molecules Targeting Human UDP-GlcNAc 2-Epimerase

Jacob L. Gorenflos López,[a, b] Gillian L. Dornan,[a] Nico Boback,[c] Martin Neuenschwander,[a] Andreas Oder,[a] Kristin Kemnitz-Hassanin,[a] Peter Schmieder,[a] Edgar Specker,[a] Hatice Ceyda Asikoglu,[a, d] Christian Oberdanner,[e] Carola Seyffarth,[a] Jens Peter von Kries,[a] Daniel Lauster,[c] Stephan Hinderlich,[d] and Christian P. R. Hackenberger*[a, b]

Uridine diphosphate *N*-acetylglucosamine 2-epimerase (GNE) is a key enzyme in the sialic acid biosynthesis pathway. Sialic acids are primarily terminal carbohydrates on glycans and play fundamental roles in health and disease. In search of effective GNE inhibitors not based on a carbohydrate scaffold, we performed a high-throughput screening campaign of 68,640 drug-like small molecules against recombinant GNE using a UDP detection assay. We validated nine of the primary actives with an orthogonal real-time NMR assay and verified their IC_{50} values in the low micromolar to nanomolar range manually.

Stability and solubility studies revealed three compounds for further evaluation. Thermal shift assays, analytical size exclusion, and interferometric scattering microscopy demonstrated that the GNE inhibitors acted on the oligomeric state of the protein. Finally, hydrogen-deuterium exchange mass spectrometry (HDX-MS) revealed which sections of GNE were shifted upon the addition of the inhibitors. In summary, we have identified three small molecules as GNE inhibitors with high potency *in vitro*, which serve as promising candidates to modulate sialic acid biosynthesis in more complex systems.

Introduction

Sialic acids are, for the most part, terminal carbohydrates on glycans. Their individual types are called neuraminic acids (Neu).[1] They are a major class of ligands for intrinsic receptors like sialic acid-binding immunoglobulin-like lectins (Siglecs) and

[a]   J. L. Gorenflos López, G. L. Dornan, Dr. M. Neuenschwander, A. Oder,
      K. Kemnitz-Hassanin, Dr. P. Schmieder, Dr. E. Specker, H. C. Asikoglu,
      C. Seyffarth, Dr. J. P. von Kries, Prof. Dr. C. P. R. Hackenberger
      Leibniz-Forschungsinstitut für Molekulare Pharmakologie (FMP)
      Robert-Rössle-Strasse 10, 13125 Berlin (Germany)
      E-mail: hackenbe@fmp-berlin.de

[b]   J. L. Gorenflos López, Prof. Dr. C. P. R. Hackenberger
      Humboldt Universität zu Berlin, Department Chemie
      Brook-Taylor-Strasse 2,12489 Berlin (Germany)

[c]   N. Boback, Prof. Dr. D. Lauster
      Freie Universität Berlin
      Institut für Pharmazie, Biopharmazeutika
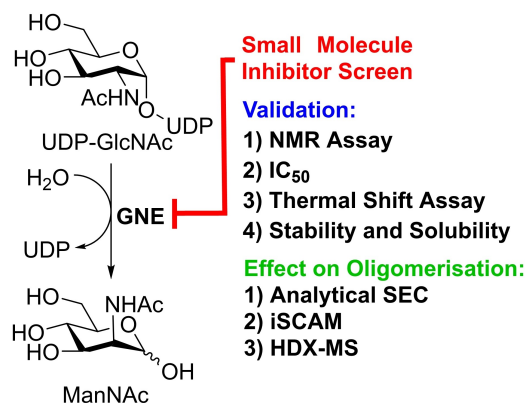   Kelchstr. 31, 12169 Berlin (Germany)

[d]   H. C. Asikoglu, Prof. Dr. S. Hinderlich
      Berliner Hochschule für Technik (BHT)
      Seestrasse 64, 13347 Berlin (Germany)

[e]   Dr. C. Oberdanner
      TECAN Group Ltd.
      Untersbergstraße 1a, 5082 Grödig (Austria)

selectins, facilitating cellular recognition.[2] Moreover, pathogenic organisms often target sialic acids due to their wide distribution and terminal location on glycans.[3] One well-known role of sialic acids is the initial binding of airway epithelium cells by hemagglutinin of influenza viruses.[4]

De novo sialic-acid biosynthesis in vertebrates is proceeded by four steps in the cytosol. The first step is conducted by the so-called "master regulator" of the sialic acid biosynthesis pathway, the uridine diphosphate *N*-acetylglucosamine 2-epimerase (GNE).[5] GNE epimerises uridine diphosphate *N*-acetylglucosamine (UDP-GlcNAc) to *N*-acetylmannosamine (ManNAc) while UDP is cleaved off (Scheme 1). GNE is one subunit of the bifunctional GNE/ManNAc kinase (GNE/MNK). MNK phosphorylates ManNAc to ManNAc-6-phosphate (ManNAc-6P). The sialic acid synthase (SAS) catalyses the formation

Scheme 1. Aim of this study: Identification and validation of small molecule inhibitors of GNE by small molecules found in a high-throughput screening.

ChemBioChem

Research Article
doi.org/10.1002/cbic.202300555

Chemistry Europe
European Chemical
Societies Publishing

of *N*-acetylneuraminic acid 9-phosphate (Neu5Ac-9P), by condensing phospho*enol*pyruvic acid (PEP) and ManNAc-6P to Neu5Ac-9P. Finally, the sialic acid phosphatase (SAP), the only non-essential enzyme of this pathway,[6] dephosphorylates Neu5Ac-9P to Neu5Ac.

In light of the biological importance of sialic acids, significant efforts have been invested since the 1990s in identifying compounds to inhibit sialic acid biosynthesis, in particular targeting GNE and MNK. So far, mainly carbohydrate derivatives have been identified. The first one was 3-*O*-methyl-GlcNAc, which was shown to inhibit MNK activity.[7] In a later study, the per-acetylated version of this carbohydrate was tested *in cellulo* and reduced cell surface sialylation could be observed.[8] Several other carbohydrate derivatives had been synthesised and tested *in vitro* but not validated *in cellulo*.[9] In 2016, we published the synthesis of a C6-Se modified *N*-acetyl mannosamine analogue and validated it as an effective MNK inhibitor *in vitro*.[10] The per-acetylated version of this compound was shown to reduce cell surface sialylation on Jurkat cells. In order to identify non-carbohydrate based molecules to interfere in the sialic acid biosynthesis pathway, we conducted a screening campaign against recombinant MNK. These efforts yielded several promising inhibitors with low μM IC_{50} values, which were validated with an independent assay.[11]

In the current study, we aimed to identify small molecule inhibitors of GNE to target an earlier enzymatic step in sialic acid biosynthesis by using state-of-the-art high-throughput screening and a panel of characterisation methods. We could obtain several potent GNE-inhibitors and identified the inhibition mechanism as interference with the oligomeric state of the enzyme (Scheme 1).

Results and Discussion

Preparation for the high-throughput screening campaign against GNE

Recombinant GNE was expressed and purified based on previously published protocols.[12] As GNE converts UDP-GlcNAc to ManNAc and UDP, we used the UDP-Glo™ luminescence assay for high-throughput screening to measure UDP release (Supplementary Figure 1). To screen for inhibitors and activators we aimed for conditions at which GNE could convert 50% of 5 μM UDP-GlcNAc to ManNAc and UDP in 1 h at room temperature. We identified 1.5 μg/mL (32.1 nM) GNE with a 1:3 diluted UDP-Glo™ (Supplementary Figure 2) assay to be the ideal concentrations (conditions are referred to as *optimised GNE activity assay*, Supplementary Figure 3A).

After verifying the activity of the known GNE-inhibitors Zn^{2+}[13] and the feedback inhibitor CMP-Neu5Ac[5] (Supplementary Figure 3B and C), and their use in the UDP-Glo™ assay, we determined the K_M of GNE for UDP-GlcNAc. For this, we used the undiluted UDP-Glo™ assay and reduced the reaction time to 20 min. In tune with the reported values,[14] the K_M was measured to be 27 ± 5 μM (Supplementary Figure 4).
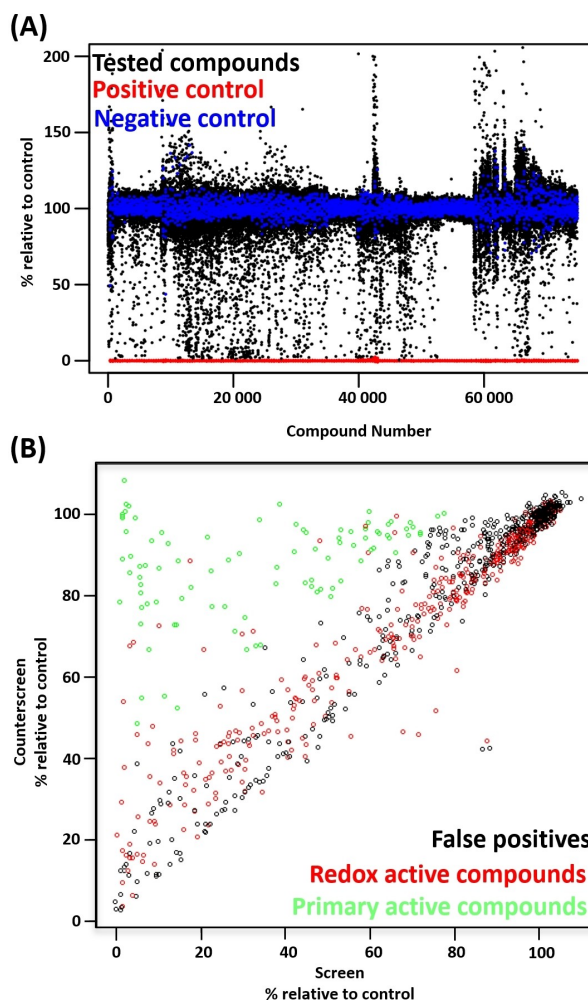

(A)

(B)

Figure 1. (A) Inhibition/activation plot for the 68,640 compounds of the *FMP screening library* tested at 10 μM in a primary screening campaign with the UDP-Glo™ assay. The compound number is an arbitrary index for visualization purposes. Positive control values are red, negative control values are blue, and sample values are black. (B) Counter screen of 1043 primary actives on 3 plates for the hit validation of primary actives. The counter screen system contained 2.5 μM UDP, to which the inhibitors were added. Black, false positives; red, redox active compounds; green, hits defined as confirmed by the counter screen.

Next, we performed the *optimised GNE activity assay* in a multi-channel/multi-step dispenser set-up, as intended for the screening campaign. We determined a Z-factor of 0.88, which we envisaged as a very good statistical outcome to start the high-throughput screening campaign (Supplementary Figure 5).[15]

First, we tested a small subset of compounds (1408 compounds including FDA-approved drugs) in duplicates. The relative activities were analysed by the Bland-Altman method, visualizing the agreement between replicates, with the aim of assessing if the employed method is suitable for an unireplicate screening campaign. For this, the relative difference between the replicates of the tested compounds was plotted on the y-axis and the mean activity of the replicates was plotted on the x-axis.[16] 95% of the measurements fell within a ± 5% of relative difference between the replicates (Supplementary Fig-
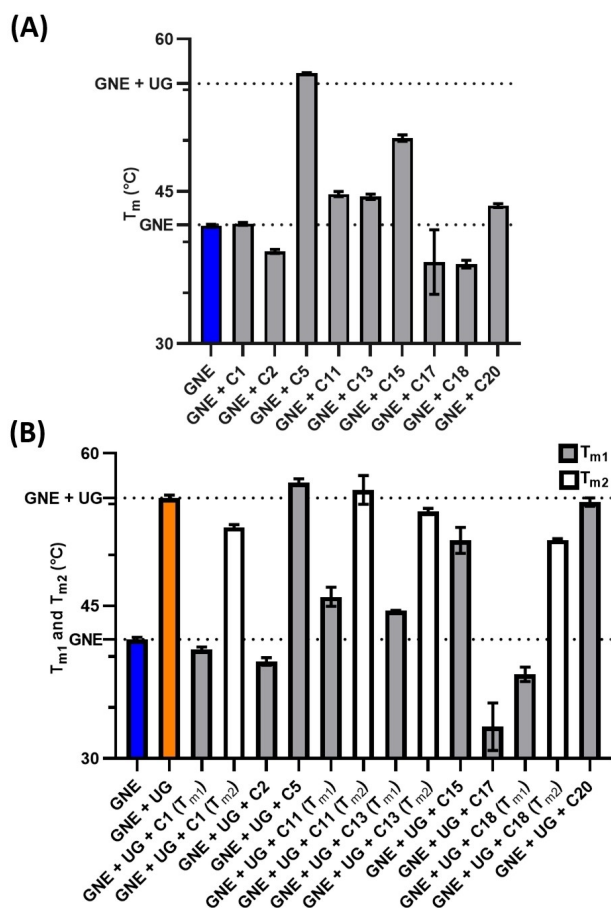
ChemBioChem

Research Article
doi.org/10.1002/cbic.202300555

**Chemistry
Europe**
European Chemical
Societies Publishing

Figure 2. (A) Tm of GNE (10 μM) in GNE buffer with GNE inhibitors (100 μM). (B) T_{m1-2} of GNE (10 μM) in GNE buffer with UDP-GlcNAc (UG – 100 μM) and GNE inhibitors (100 μM).

Figure 3. Analytical size exclusion chromatography (aSEC) of GNE (16 μM) with different ligands (100 μM). The samples were pre-incubated with the compounds for 5 min at 4 °C. (A) Control experiments displayed in all following figures. (B) aSEC with C5. (C) aSEC with C13. (D) aSEC with C15.

ure 6A). This high degree of agreement is also visible for most active samples that deviate from the background, with only a few exceptions.

In 2017, a similar screening campaign from our group had been conducted against the kinase domain MNK of the bifunctional GNE/MNK,[11] during which we identified 174 primary active inhibitors. For the current project, the 174 primary actives were tested in a counter screen with the *optimized GNE activity assay* using 20 μL per well of GNE buffer with 2.5 μM UDP. Small molecules that inhibit the UDP-Glo™ assay displayed the same results in the counter-screening as in the screening conditions. No primary active against MNK had any significant activity against GNE (Supplementary Figure 6B).

High-throughput screening campaign against recombinant GNE

Next, we screened a total of 195 assay plates (384-well) containing 68,640 compounds, in which the final compound concentration was 10 μM. The assay showed a good signal separation with a median Z-factor of 0.86 over all plates. None of the plates had a Z-factor below 0.5. An overview plot
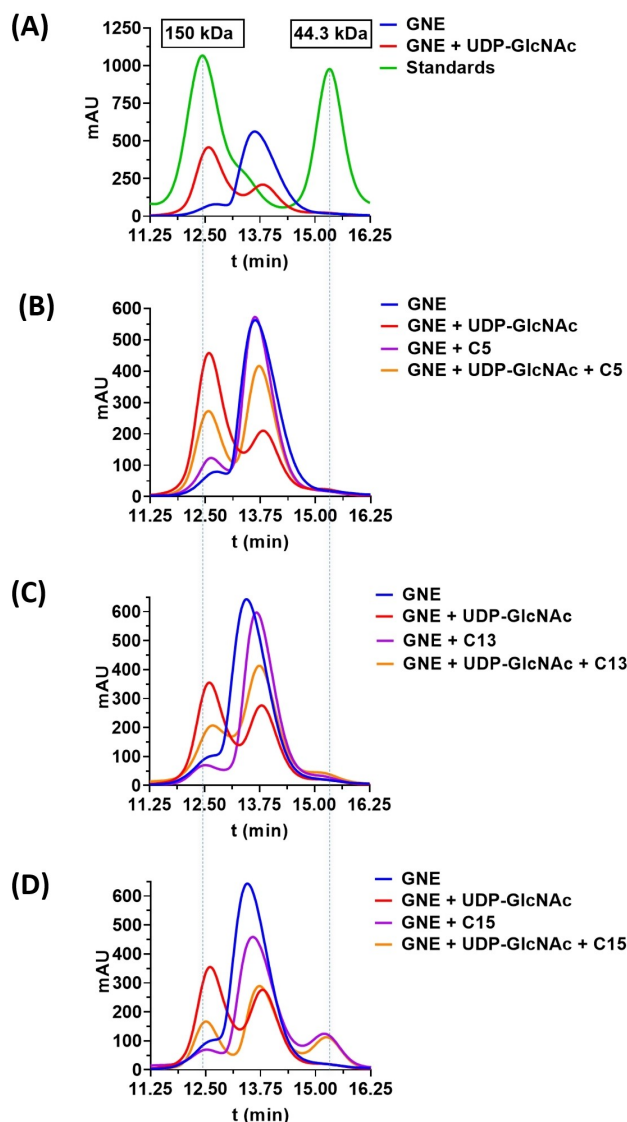
depicting the relative activities of all measured samples is shown in Figure 1A. Signal separation remained constant throughout the screen. Activated and inhibited samples were distinguishable from the inactive background. The z-score distribution of the samples presented the expected Gaussian-like distribution, showing successful normalization of the signal across the plates (Supplementary Figure 7). For the hit selections, samples which significantly decreased luminescence, starting with a z-score smaller than 4 and a decreased luminescence of at least 50%, were selected. The resulting 1043 hits were picked into three 384-well plates to be analysed in a counter screen with 2.5 μM UDP. False-positive hits gave comparable results in the counter screen and in the screening set-up. As such, they were identified on the diagonal of the counter-screen plot (Figure 1B). An enrichment analysis of potentially unfavourable properties in primary actives showed
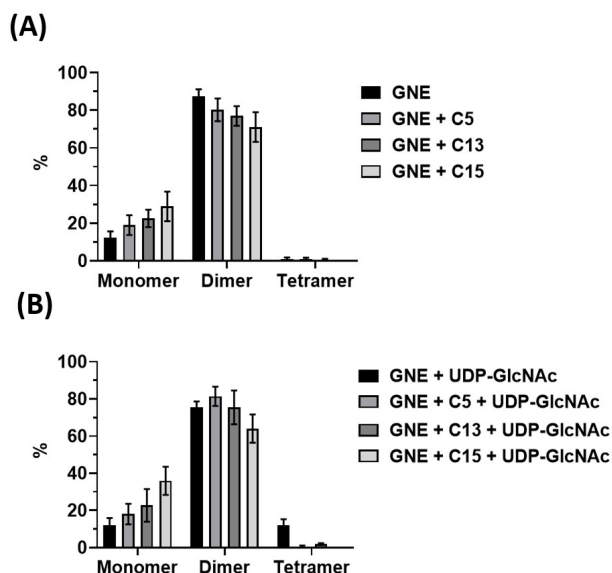
ChemBioChem

Research Article
doi.org/10.1002/cbic.202300555

Chemistry Europe
European Chemical
Societies Publishing

(A)

(B)

Figure 4. iSCAM measurements of the oligomeric state of GNE at 431 nM in (A) absence of UDP-GlcNAc or (B) presence of UDP-GlcNAc. In both conditions different inhibitors (10 μM) were compared to a non-treated control. The error bars indicate the standard deviation with $N = 4$ independent measurements. Each measurement detected around 4000 counts.

significant enrichment of redox active compounds (Supplementary Figure 8; also indicated in Figure 1B), hence the hits were tested for redox activity with a Resazurin/Resorufin assay.[17] 105 compounds showed favourable activities in the counter screen and did not show positive activity in the redox assay. They were picked into a 384-well plate and serially diluted in a range of 0.1–100 μM. In parallel, compound activities were tested in a concentration-dependent counter screen without GNE. The threshold of the hit selection was set to a 75% reduction of GNE activity together with a sigmoidal curve shape. For the counter screen, an IC_{50} by one order of magnitude greater than the IC_{50} found in the screen was set as selection criteria (Supplementary Figure 9). Furthermore, this selection step was combined with frequent hitter exclusion. Frequent hitters were defined if they were found more than five times in all primary biochemical screening campaigns conducted with the FMP-compound library. 34 compounds fulfilled these criteria. Finally, the 34 remaining GNE inhibitors were analysed by HPLC-MS regarding their purity and their ability to chelate Zn^{2+} ions, since earlier experiments had demonstrated that Zn^{2+} inhibits GNE activity at nM concentrations (Supplementary Figure 3C).[13] Zn^{2+} chelators were identified by the annotation in the screening library. A flow chart illustrating the whole selection and screening process is given in Supplementary Figure 10.

In total, 28 GNE inhibitors could be identified, which are displayed in Supplementary Figure 11. To facilitate further description of the compounds, they were listed by ascending FMP-library code and numbered from 1 to 28. Of these, 12 were purchased based on availability and further analysed.

Primary active validation

The primary hits were validated with a plate reader-independent and orthogonal NMR-assay.[18] The *N*-acetyl methyl of UDP-GlcNAc and ManNAc were found to display characteristic chemical shifts around 2.1–1.9 ppm (Supplementary Figure 12). By recording these spectra in regular intervals, the conversion of UDP-GlcNAc to ManNAc could be monitored in real-time by NMR (Supplementary Figure 13). An HSQC spectrum of the end-product verified that ManNAc had been formed (Supplementary Figure 14). 4 μg/mL GNE were found to efficiently convert 200 μM UDP-GlcNAc over the course of 16 h (Supplementary Figure 15A). To validate the assay, the known inhibitors CMP-Neu5Ac and Zn^{2+} ions were used (Supplementary Figure 15B).

The compounds varied in their GNE inhibition potency and were categorised for complete inhibition, partial inhibition, and no inhibition. Compound C7, C10 and C21 were found to have no inhibition effect on GNE, whereas C5, C11, C13, C15 and C20 inhibited GNE partly and C1, C2, C17 and C18 completely inhibited GNE (Supplementary Figure 15C–D). The validated inhibitors were manually retested with the *optimised GNE activity assay*. The results were found to be in line with the previously determined IC_{50} values (Table 1 and Supplementary Figure 16).

To validate that the inhibitors bound to GNE a thermal shift assay with up to 96 conditions was conducted. GNE (10 μM) was found to have a melting point T_m of 41.7 °C (Supplementary Figure 17). The addition of UDP-GlcNAc increased the T_m by 13.9 K to 54.6 °C (Supplementary Table 2), indicating that the substrate binding induced a massive shift in the protein structure towards higher stability. We speculated that this could be the formation of the homodimer of dimers described by Ghaderi *et al.*[19] for the full length GNE/MNK. Surprisingly, CMP-Neu5Ac did not induce a similar effect, although it stabilised

Table 1. Inhibitory potency of 12 GNE inhibitors validated by the RT-NMR assay, the IC50 values found in the screening campaign and the IC50 values of the purchased compounds, which were re-analysed manually.

Compound	Inhibition in RT-NMR assay	IC_{50} (μM) (Screening campaign)	IC_{50} (μM) (Manual re-testing)
C1	Complete	9.1	7.6
C2	Complete	8.9	1.9
C5	Partial	3.1	3.1
C7	None	n.d.	n.d.
C10	None	n.d.	n.d.
C11	Partial	3.9	9.9
C13	Partial	7.9	2.4
C15	Partial	1.9	0.39
C17	Complete	0.043	0.132
C18	Complete	9.7	2.5
C20	Partial	10	19
C21	None	n.d.	n.d.

ChemBioChem

Research Article
doi.org/10.1002/cbic.202300555

Chemistry Europe
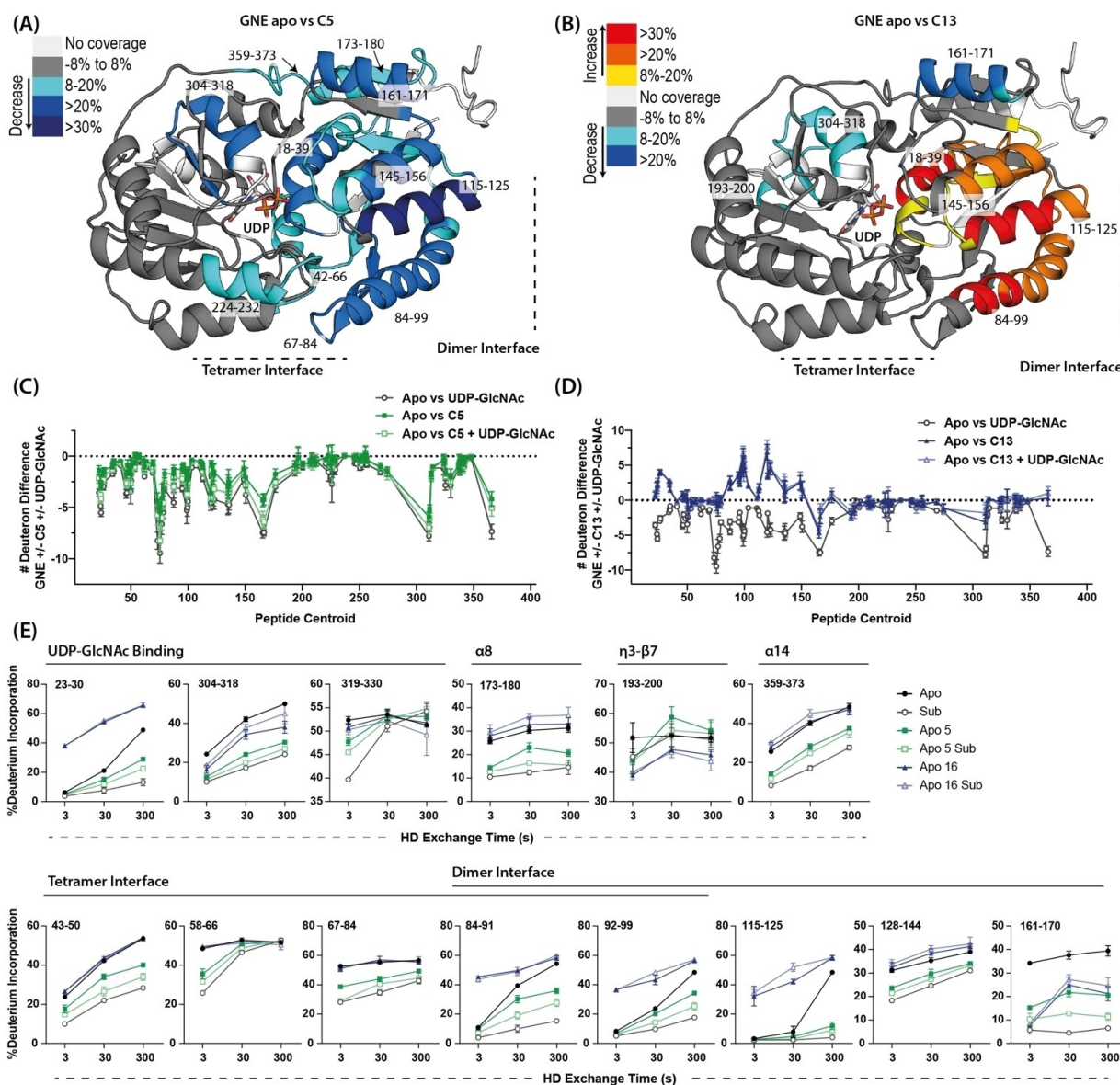European Chemical
Societies Publishing

Figure 5. Hydrogen-Deuterium Exchange Mass Spectrometry of GNE (500 nM) with different ligands (50 μM) and/or UDP-GlcNAc (5 μM). (A) Differences in deuterium incorporation between apo GNE compared with GNE in complex with C5 or C5 and UDP-GlcNAc mapped onto the structure of GNE (PDB:4ZHT) (B) Differences in deuterium incorporation between apo GNE compared with GNE in complex with C13 or C13 and UDP-GlcNAc mapped onto the structure of GNE (PDB:4ZHT) (C) # Deuteron differences across all time points for GNE apo compared with GNE bound to C5 and/or UDP-GlcNAc along the primary sequence of GNE. (D) # Deuteron differences across all time points for GNE apo compared with GNE bound to C13 and/or UDP-GlcNAc along the primary sequence of GNE. (E) % Deuterium incorporation across time for representative peptides from different regions of GNE for all conditions.

the protein structure beyond the initial 13.9 K, if incubated together with UDP-GlcNAc (Supplementary Table 2).

In a first set of experiments with the inhibitors alone, GNE (10 μM) was incubated with 100 μM of the respective inhibitors (Figure 2A). C11, C13, C15, and C20 significantly increased GNE stability. C5 even increased protein stability beyond the effect of UDP-GlcNAc. C2, C17, and C18 decreased GNE stability and C1 did not change it. Afterwards, these experiments were repeated in the presence of UDP-GlcNAc (100 μM) (Figure 2A). The results for C2, C5, C15, and C17 were for the most part unchanged. C20 with UDP-GlcNAc had a thermal shift like GNE with UDP-GlcNAc. Unexpectedly, the addition of the substrate

of GNE resulted in the emergence of two distinct states (Supplementary Figure 18) with different thermal shifts for the compounds C1, C11, C13, and C18 (Figure 2B and Supplementary Table 2). The first thermal shift was labelled T_{m1}, and the second thermal shift was labelled T_{m2}. These experiments demonstrate that all validated inhibitors in fact bound to GNE and likely influenced its structure.

ChemBioChem

Research Article
doi.org/10.1002/cbic.202300555

Chemistry Europe
European Chemical
Societies Publishing

Table 2. Stability of 50 μM GNE inhibitors in serum free cell culture medium at 4°C and 37°C, and solubility of GNE inhibitors (100 μM) in serum free cell culture medium after 60 min incubation at room temperature.

Compound	Stability at 4 °C	Stability at 37 °C	Solubility at 100 μM
C1	Stable	Unstable	/
C2	Unstable	Unstable	/
C5	Stable	Stable	Soluble
C11	Stable	Stable	Insoluble
C13	Stable	Stable	Soluble
C15	Stable	Stable	Soluble
C17	Stable	Partially stable	/
C18	Partially	Unstable	/
C20	Unstable	Unstable	/

Scheme 2. Chemical structures of the validated, serum stable and soluble GNE inhibitors found in the screening campaign.
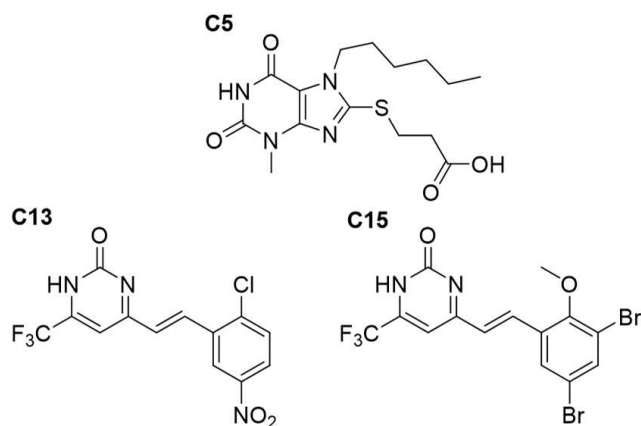
The stability and solubility of the tested GNE inhibitors

Next, we tested the nine remaining GNE inhibitors for stability and solubility in serum-free cell-culture medium. Compound stability at 4°C and 37°C was monitored by UPLC-UV (Supplementary Figure 19). For the experiment at 4°C the sample holding chamber was cooled and aliquots of the same vial were taken after 3, 6, 12, 18, 24/29, and 48 h. In parallel, endpoint measurements (72 h of incubation only) were conducted after incubation at 37°C to mimic experimental conditions in a cellular assay. The compounds were analysed based on their relative extinction at 220 nm and the results categorised as stable, partially stable (peak intensity between 30% and 100% of the initial signal) and unstable (peak intensity below 30% of the initial signal). The ester-containing compounds C2, C18, and C20 were evaluated as unstable at both temperatures. Ester C18 showed a plateau at 4°C after an initial decrease (Supplementary Figure 20) and complete cleavage at 37°C (Supplementary Figure 21). The nitril containing compounds C1 and C17 were both stable at 4°C but not at 37°C. As such, only the four nucleoside analogues (purine derivative C5 and pyrimidinone derivatives C11, C13, and C15) revealed stability at 4°C and 37°C (Table 2).

The compounds' solubility was analysed by microscopy detection of precipitates. Compounds C5, C11, C13, and C15 were analysed in concentration ranges from 12.5 μM to 100 μM, since their IC_{50} values were below 12.5 μM. The samples were measured at 0 min and 60 min. Only C11 showed significant insolubility starting at 25 μM (Table 2 and Supplementary Figure 22A–B).

C5, C13, and C15 inhibit the oligomerisation of GNE

As a result of the stability and solubility studies, only three GNE inhibitor candidates remained (Scheme 2). We aimed to further characterise their effect on the oligomeric state of GNE. The data obtained from the thermal shift assay experiments indicated that the GNE subdomain exists in two distinct states,[19] since the addition of the substrate UDP-GlcNAc led to a significant shift in Tm (Figure 2B). For full-length GNE/MNK, these states were postulated to be the homodimer form of GNE, and the homodimer of dimers that formed upon addition of the substrate UDP-GlcNAc.[19] Analytical size exclusion chromatography (aSEC) of GNE revealed one main peak of GNE (13.75 min, 93 kDa), representing the dimer. The addition of UDP-GlcNAc led to a second peak (12.50 min, 186 kDa) which fits the homodimer of dimers (Figure 3A; see also Supplementary Figure 23A for full length chromatogram). Similar effects were observed with UDP. Surprisingly, CMP-Neu5Ac did not induce tetramer formation (Supplementary Figure 23B).

The GNE inhibitors C5, C13, and C15 were tested with aSEC for their effect on the oligomeric state of GNE. For all compounds tetramer rearrangement by UDP-GlcNAc incubation was strongly reduced, indicating that the validated GNE inhibitors affected the oligomeric state of GNE, and its enzymatic activity by an altered ratio of the enzymatically active tetramer to the inactive dimer. Interestingly, under these conditions C5 partially induced the formation of the GNE tetramer without presence of UDP-GlcNAc (Figure 3B). In contrast, C15 induced a third GNE species, appearing to be the GNE monomer. In the thermal shift assay experiments C15 increased T_{m1} of GNE from 41.7°C to over 50°C, without and with UDP-GlcNAc, respectively (Figure 2B).

Next, we used interferometric scattering microscopy (iS-CAM) to have a state-of-equilibrium experiment for validation inhibitor effects on GNE with and without UDP-GlcNAc preincubation at room temperature. iSCAM represents a sensitive label-free microscopy technique, based on the interferometric pattern of scattered light at nanoobjects such as proteins and reflected light at the glass-water interface.[20] As such, we envisioned that this technique would be perfectly suited to study the changes in the oligomeric state of GNE upon addition of the GNE inhibitors. Surprisingly, we identified a sizeable proportion of monomeric proteins at steady-state conditions, which were not detectable from experiments using

ChemBioChem

Research Article
doi.org/10.1002/cbic.202300555

Chemistry
Europe
European Chemical
Societies Publishing

analytical SEC. (Figure 4A and Supplementary Figure 24A). The addition of UDP-GlcNAc increased the tetrameric population, while the abundance of monomers maintained unchanged. This finding validates the hypothesis that the tetrameric population is formed by the interaction of two GNE dimers by UDP-GlcNAc incubation. However, tetramer formation was completely inhibited by all inhibitory compounds (Figure 4B and Supplementary Figure 24B). Furthermore, C13 and C15 act on GNE by disrupting the dimeric state. This observation of monomer formation was exclusive for iSCAM experiments.

To get more insight into how these compounds affected the oligomeric state of GNE on a protein structure level, we used hydrogen-deuterium exchange mass spectrometry (HDX-MS), which measures the exchange rate of amide hydrogens in solution (Figure 5, Supplementary Figure 25, Supplementary Data File). HDX-MS can therefore provide information about a protein's structure and dynamics.[21] Due to the complexity of HDX-MS experiments, only C5 and C13 were investigated. GNE was incubated with the inhibitors or DMSO blank before further incubation with UDP-GlcNAc or water blank. GNE incubated with UDP-GlcNAc alone showed results that complimented the existing crystal structure.[12] Large decreases in exchange rates were observed throughout the primary sequence of GNE in regions that form the dimeric or tetrameric interfaces as well as in regions that are involved in substrate binding (Figure 5E, Supplementary Figure 25f).

Addition of C5 led to decreases in exchange rates across GNE in similar regions as observed for UDP-GlcNAc, although these changes were fewer and not as large as those induced by substrate UDP-GlcNAc alone (Figure 5A, C, E). Therefore, it appears that C5 leads to conformational changes similar to substrate binding, potentially leading to oligomerisation of GNE. These effects were enhanced upon incubation with C5 followed by UDP-GlcNAc, indicating that the compound is unlikely to bind to and occlude the substrate binding site. Some of the substrate binding regions did not have decreases in exchange that met experimental thresholds when GNE was incubated with C5 alone or C5 together with a substrate (218–232, 252–261 & 319–332). It is possible that binding of C5 leads to conformational changes that impair but do not abrogate substrate binding completely. There were no unique regions of decreased deuterium exchange in the C5 samples, therefore it is difficult to ascertain the exact binding region of this compound.

Addition of C13 alone revealed striking increases in exchange in regions associated primarily with the dimer interface of GNE, indicating the potential for this compound to disrupt the natural oligomeric state of GNE (Figure 5B, D, E). Few areas of decrease were observed, however one of these regions is in close proximity to the dimer interface (161–171) and one area that is involved in substrate binding (304–318). These could be the binding interfaces of C13. Further increases were seen in a region of substrate binding (18–38) and incubation with both UDP-GlcNAc and C13 showed similar trends as C13 alone, indicating that the binding of C13 might also alter the ability of UDP-GlcNAc to bind to GNE and initiate

tetramerization or that C13 abrogation of the dimer state impairs tetramerization by the substrate.

Conclusions

In this study, a screening campaign of 68,640 small molecules against recombinant GNE was conducted. Of 28 actives identified in a primary screen and concentration-dependent validation using a luminescence-based high-throughput assay, nine compounds with promising primary actives were validated with a screening-method independent real-time NMR spectroscopy assay. Due to instability and insolubility in cell-culture medium of six compounds, only three small molecules were further analysed. These three compounds showed IC_{50} values in the low μM range and have structural relationship to nucleobases. C5 a derivative of the purine base xanthine, C13 and C15 are pyrimidinone derivatives. The latter fit with the hypothesis of Blume et al., who suggested the UDP moiety as an essential part of effective GNE inhibitors.[22] It is therefore very likely, that the compounds address the active site by competitive effects.

Former studies[14a,19] revealed, that the allosteric inhibitor CMP-Neu5Ac, and in particular the substrate UDP-GlcNAc, stabilize the GNE-active tetrameric state of the bifunctional GNE/MNK. In addition, UDP-GlcNAc is able to reassociate the tetramer from a partially inactive GNE/MNK dimer. Recombinant GNE used for the screening campaign mainly exists as an inactive dimer (see e.g. Figures 3A and 4 A). The screening assay with UDP-GlcNAc therefore does not only reflect the enzymatic activity, but also the reassociation of the GNE tetramer. We therefore investigated the compounds by biophysical methods, indicating their influence on the oligomeric state of GNE. Homogenous trends with regard to oligomerisation could be observed in thermal shift assays, aSEC and iSCAM for compounds C13 and C15, indicating the inhibitory mechanism of these compounds preventing reassociation of the GNE tetramer, most likely by blocking the active site for UDP-GlcNAc binding. These data are underlined by HDX-MS, which showed strong structural influence of C13, leading to disruption of the native oligomeric state.

For the compound C5, thermal shift assays and to a lesser extent aSEC data suggested that C5 induced the opposite effect, since this compound is able to form GNE tetramers. HDX-MS measurements further pointed to this assumption, although the experimental conditions are different (GNE concentration was more than 10-fold lower in HDX-MS compared to the other two methods; HDX-MS was conducted at 23 °C, aSEC at 4 °C and thermal shift assays between 25 and 99 °C). These findings suggest a potential role of C5 as a mimic of UDP-GlcNAc, the native GNE substrate, which is highly effective in tetramer association (see Figure 3A). Although C5 is less effective in tetramer formation, activation of GNE enzymatic activity could be expected. However, we observed inhibition of GNE by C5. Besides the structural effects, C5 could additionally act competitively to UDP-GlcNAc in the enzymatic mechanism. Further studies are therefore needed to clarify the detailed inhibitory mechanism(s) of the compounds.

ChemBioChem

Research Article
doi.org/10.1002/cbic.202300555

**Chemistry
Europe**
European Chemical
Societies Publishing

iSCAM showed a different picture of the oligomeric state of GNE and found that C5 inhibited oligomerisation and induced the formation of a monomer. Interestingly, iSCAM GNE monomers are observed in all experiments (Figure 4). This could be due to the used GNE concentration, which is more than one magnitude lower than in thermal shift assays and aSEC. Nevertheless, monomeric species were already observed for GNE/MNK by high-resolution analytical ultracentrifugation. We could not completely rule out that these species are artifacts of the recombinant proteins. Furthermore, the measurements were conducted at different temperatures chosen to yield optimal results with the respective methods. These conditions may also have effects on the oligomeric state of GNE. However, it is likely, that the observed changes in GNE oligomerization display a part of the complex regulation mechanism of GNE and GNE/MNK, respectively: fully active tetramer – partially/MNK active dimer – inactive monomer.[19] This could be influenced by the analysed compounds and underline their potential as effective inhibitors of sialic acid biosynthesis.

As a next step, after having determined how and where our newly identified small molecule inhibitors bind to GNE, we plan to further optimise them to increase potency, specificity, and intracellular stability. We envision that the resulting compounds will be instrumental in studying and manipulating sialic acid biosynthesis in biological environments, which may even provide new therapeutic potential if cell-surface sialylation can be modulated without impairing cell survival.

Experimental Section

GNE expression and purification

The GNE domain of human GNE/MNK was expressed according to a protocol published by the Chen Group.[12] The gene encoding the UDP-GlcNAc 2-epimerase domain with an *N*-terminal His6-tag was bought from Biocat in a pET21a(+). The plasmid was codon optimised to be expressed in *E. coli* BL21 (DE3) cells. The transformed BL21 (DE3) cells were stored as a glycerol stock (5%). Starting from this glycerol stock an over-day culture was grown in 5 mL LB medium with 100 mg/L ampicillin, for 8 h at 37°C and 220 rpm. From the over day culture an overnight culture was grown in 15 mL LB medium with 100 mg/L ampicillin, at 37°C and 220 rpm. With 3.5 mL overnight cultures 4×500 mL LB medium with 100 mg/L ampicillin in 2 L flasks were inoculated. This was grown at 37°C and 180 rpm to $OD_{600} = 1.9$. Then all cultures were pooled, and 700 mL were diluted in 1.3 L LB medium with 100 mg L^{-1} ampicillin (at 4°C). This was redistributed to four 2 L flasks (4×500 mL), grown to $OD_{600} = 0.7$ and induced with IPTG (50 μM). Subsequently, the cells were kept for 42 h at 8°C and 120 rpm. Then they were grown for 24 h at 16°C and 180 rpm. The cells were harvested by centrifugation with 4000 g for 15 min at 4°C and the cell pellet was re-suspended in resuspension buffer (50 mM Tris-HCl, pH 8.0, 500 mM NaCl). The cells were lysed by micro fluidizing at 18 kpa (Microfluidics – LM10). The cell lysate was centrifuged with 20 000 g for 25 min at 4°C. The clarified supernatant was filtered, and the protein was purified *via* Ni-NTA chromatography on 2×5 ml His60 Ni Superflow column – (Takara/Clontech) by a Biorad-NGC™ Chromatography System utilizing resuspension buffer and elution buffer (50 mM Tris-HCl pH 8.0, 500 mM NaCl, 500 mM Imidazole) in a linear gradient over 300 mL. Fractions of the protein

peak were pooled and concentrated to 10 mL using a Vivaspin 20 (Sartorius) with a molecular weight cut of at 10 kDa. The sample was then re-buffered to 50 mM Tris-HCl, pH 8.0, 100 mM NaCl, 5% glycerol and 0.2 mM TCEP using a HiPrep 26/10 Desalting column (GE Healthcare) on a Biorad-NGC™ Chromatography System. Fractions containing the GNE protein were pooled. 20 mL with a concentration of about 7 mg/mL were obtained.

Compound library

A library of 68,640 compounds was tested at the Screening Unit core facility of the FMP. The library consists of a 30,976-member diversity set that was designed on the basis of the maximum common substructure principle,[23] 4576 fragments containing carboxyl and amine groups, 3,168 compounds with known pharmacological activity (Library of Pharmacologically Active Compounds, LOPAC, Sigma-Aldrich) and FDA- approved drugs or drug candidates (Selleckchem), 704 compounds derived from known ChEMBL targets, 20,064 compounds with natural product derived scaffolds from AnalytiCon Discovery GmbH and a further set of 9,152 compounds submitted by academic groups. The screening libraries are arranged in 384-well plate format, in which compounds are plated into columns 1 to 22. The compounds are initially dissolved in DMSO at a concentration of 10 mM and are further diluted in DMSO to a concentration of 1 mM in compound mother plates Columns 23 and 24 served as free spaces for the addition of controls. Thus 352 compounds can be screened per plate with 32 controls.

High-throughput luminescence GNE assay

Measurements were conducted in the following assay buffer unless noted otherwise: Tris·HCl (pH 8, 50 mM), NaCl (100 mM), Tween 20 (0.005% v/v), BSA (0.05%), TCEP (0.2 mM), Glycerol (5%). UDP-GlcNAc was applied at a final concentration of 5 μM and GNE was applied at a final concentration of 32 nM (1.5 μg/mL). Substrate and enzyme stock solutions were prepared in assay buffer. UDP-GlcNAc substrate solution (2-fold concentrated, 10 μL) was dispensed into a white polystyrene 384-well microplate (3574, Corning) into columns 1–24. Compounds (200 nL each) were transferred from the 384-well mother plates to the assay plate by use of a Tecan Evo robotic liquid handler equipped with a 384-channel fixed-tip pipetting head (Tecan AG, Männedorf, Switzerland). GNE (2-fold concentrated, 10 μL) was dispensed into columns 1–23, and assay buffer (10 μL) was added as negative control (no enzyme activity) to column 24. In column 23 positive control samples only receiving DMSO were present (=100% enzyme activity). This procedure resulted in a final reaction volume of 20 μL and a compound concentration of 10 μM for primary screening with use of mother plates with 1 mM compound solutions. The assay plates were incubated at room temperature for 1 h. UDP-Glo assay reagent (Promega) that had been diluted 1:3 (10 μL) was dispensed into columns 1–24, the plates were incubated for another 1 h at room temperature, and luminescence signals were finally read out with an EnVision Reader (PerkinElmer).

Counter screenings for inhibitors and activators

For direct assay interference, luminescence assay buffer containing UDP (2.5 μM for inhibitor counter screening and 5 μM for activator counter screening) was prepared (thereby a reaction run to 50% and 100% completion, respectively, was simulated) and dispensed into columns 1–23. Column 24 contained assay buffer without UDP. Compound solutions (200 nL) were transferred from cherry-picked plates containing compounds at a concentration of 1 mM in DMSO,

resulting in a final compound concentration of 10 μM in the assay buffer.

Concentration-dependent screen of inhibitors

For assessing up to 352 samples, compounds showing activity after primary screening were distributed from stock solutions (10 mM in DMSO) to a 384-well plate into columns 1–22 in 5 μL aliquots. Serial dilutions of the compounds were conducted by adding DMSO (5 μL) to the compound samples, mixing and transferring the diluted sample (5 μL) to an empty plate. Nine consecutive two-fold serial dilutions across the plates were generated by use of a 384-channel fixed- tip pipettor (TeMO384, Tecan). For assessing up to 32 samples, concentrated stock solutions (5 μL) were arranged into columns 1 and 12 of a 384-well plate, and 11 consecutive serial twofold dilutions were pipetted across the columns within the plate by use of a 384-channel disposable tip pipettor with 1 column of tips mounted. Then, exactly the same method as for the luminescence assay was used as in primary screening by transfer of compound (200 nL), with duplicate measurements for each plate.

Real time NMR assay

Experiments were conducted in the same buffer as the high-throughput luminescence GNE assay. The UDP-GlcNAc and the GNE inhibitors were diluted in reaction buffer to their final 2x concentrations. Recombinant enzymes were also diluted in reaction buffer to their final 2x concentrations. 5% of one of these cocktails was set up to be D_2O. The reactions were started by mixing the two aforementioned 2x solutions to a final volume of 600 μL and transferring this reaction cocktail to an NMR tube. The sample holder and the spectrometer were set to the same temperature if the sample temperature was 295 K. Reaction kinetics were slow at this temperature and samples were shuttled between the NMR spectrometer and the sample holder. Four experiments were recorded per hour, which were repeated 16 times. A specific number of experiments in regularly interspaced intervals with a defined start time was set up. The specified start time allowed to pre-mix the reaction components at a pre-defined time point, ensuring consistent reactions throughout experiments. In this study, all reactions were started 2 min before the time point zero measurements. To ensure that all experiments fit in their allotted time frame, extensive experiments were conducted for each method, testing the speed at which samples are processed once they are placed in the sample holder. Several standard configurations were set to speed up the pre-acquisition time. Temperature handling was turned off, which necessitated the same temperature for the pre-mixed sample, the sample holder, and the sample temperature – if this requirement was not met, signals became most inconsistent throughout an experiment. Standard gradient shimming was performed right after sample insertion. Tuning and matching were turned off for all experiments. The number of dummy scans was set to 4, and P1 pulses were determined for the used buffer and pre-set accordingly. ^{1}H-NMR experiments were run with 96 scans on a 600 MHz spectrometer. For analysis, the 1D spectra were stacked into pseudo 2D of up to 32 fids using the Bruker-script "fidtoser". Data was zerofilled to a size of 16k in f2 (the acquisition dimension). The final signal was created by integrating a fixed number of columns always using the same spectral range for the integration. These data were converted to asci format using an in-house script and plotted using GraphPad Prism 8.

Thermal Shift Assay

The samples were prepared on ice. GNE concentration was adjusted to 10 μM (464 μg/mL). UDP-GlcNAc and GNE inhibitor concentrations were adjusted to 100 μM. The final volume of each sample was set as 25 μL, which also contained 2 μL of SYPRO Orange (Sigma), that had previously been diluted 1:79 in GNE buffer. The dilutions were pipetted into a clear non-skirted qPCR-plate (BRAND), covered with an adhesive UV compatible seal and spun down with 1000 g for 5 min. The experiment was performed with the StepOnePlus™ Real-Time PCR-System (Applied Biosystems). A Fast gradient was run at 0.5% (0.71 K/min) from 25°C to 99°C. The experiment is set up to run in triplicates or quadruplicates. Only the control samples GNE and GNE-buffer (which does not contain protein) were run in octuplicates. The data was analysed with the StepOnePlus™ software. The thermal shifts were determined using the derivative reporter. If more than one thermal shift was detected, they were numbered in increasing order starting with the lowest temperature. The data was plotted using GraphPad Prism 8.

Stability of Small Molecules in DMEM

Compound stability was measured with the help of a UPLC®-UV ACQUITY H-class instrument (Waters Corporation, Milford, Massachusetts, USA) equipped with an ACQUITY UPLC®-BEH C18 1.7 μm, 2.1×50 mm column (Waters Corporation), applying a flow rate of 0.6 mL/min and using eluents A (99.9% H_2O, 0.1% TFA) and B (99.9% ACN, 0.1% TFA). UPLC-UV chromatograms were recorded at 220 nm and the small molecules were eluted with the following gradient: 0–0.5 min (5% B), 0.5–3 min (5% to 95% B), 3–4 min (95% B) and 4–5 min (5% B). The 10 mM of the compounds dissolved in DMSO were diluted 1:200 in DMEM F12. 5 μL of each sample was injected per measurement. The experiments were recorded at 0 h, 3 h, 6 h, 12 h, 18 h, 24 h and 48 h at 4°C. The data was extracted as ASCII files and plotted in Prism 8.

Solubility of GNE Inhibitors in DMEM F12

DMEM F12 was filtered with 0.2 μm filters. The compounds C5, C11, C13, and C15 in 10 mM stock solutions were diluted accordingly in this medium, adjusting a final concentration of 1% DMSO. DMEM F12 with 1% DMSO was prepared as the negative control. The serial dilutions were pipetted into a black clear bottom 384 well plate (Corning – 3762) and the plate was spun down for 1 min at 1000 g. Bright field microscopy using the 4x objective of the TECAN Spark Cyto in the indicated intervals yielded images of the well bottoms. Precipitate was identified using the confluency analysis provided by the TECAN ImageAnalyzer software. Data was plotted with Prism 8.

Size Exclusion Chromatography

All steps were conducted at 4°C. 500 μL of GNE (16.1 μM, 747 μg/mL) were incubated with 5 μL (10 mM stock solution) of carbohydrate and/or other small molecules for 5 min at 4°C. 400 μL of this sample were directly injected onto an Increase Superdex 200 increase column 10–300 GL (GE healthcare) on an Äkta pure 25. The column was preequilibrated 100 mM Tris, 50 mM NaCl, 5% glycerol, pH 8) and the samples were eluted with 1.5 column volumes of the same buffer at a flow rate of 0.75 mL/min and detected at 280 nm. A protein standard mix of 15–600 kDa (69385-6x39MG, Sigma-Aldrich) was used for calibration. Data of the individual runs were exported as ASCII files and plotted with Prism 8.

ChemBioChem

Research Article
doi.org/10.1002/cbic.202300555

Chemistry
Europe
European Chemical
Societies Publishing

Interferometric light scattering microscopy

iSCAM was measured with an OneMP from Refeyn equipped with a 525 nm laser. The instrument was supported by an Accurion (i4 Series) active vibration isolator. Reaction solutions of GNE (431 nM) and the inhibitors (10 μM) with and without UDP-GlcNAc (10 μM) were prepared in DPBS (−|−). The components were pre-incubated for 15 min at room temperature. Immediately before the measurements, the samples were diluted by a factor of 8 with DPBS (−|−). Samples (5 μL) were loaded onto the coverslip by mixing into a buffer droplet (15 μL). All measurements were performed in a regular field of view and by using the auto-focus function. The measured contrasts were referenced to protein standards using the NativeMarkMT (ThermoFisher). The data was plotted using Graph-Pad Prism 8.

Hydrogen-Deuterium Exchange Mass Spectrometry (HDX-MS)

Deuterium-Exchange Reactions

GNE apo was compared to GNE in the presence of UDP-GlcNAc and/or compounds. GNE was first mixed with compounds (C5 or C13) or a DMSO blank and incubated on ice for 10 minutes, followed by mixing with UDP-GlcNAc or water blank before incubation on ice for a further 10 minutes with final concentrations: GNE (5 μM), UDP-GlcNAc (50 μM), GNE inhibitors (500 μM) and buffer (20 mM Tris, pH 8, 100 mM NaCl, 5% Glycerol). From these mixtures, 5 μL were taken and allowed to equilibrate to room temperature for 1 min before addition of 45 μL deuterated buffer (20 mM Tris pH 8, 100 mM NaCl, 96.2% Deuterium Oxide) for 3, 30, or 300 s at RT with final concentrations: GNE (500 nM), UDP-GlcNAc (5 μM), GNE inhibitors (50 μM) and buffer (20 mM Tris, pH 8, 100 mM NaCl, 0.5% Glycerol, 86.5% Deuterium Oxide). Reactions were stopped by the addition of 20 μL of quenching buffer with final concentration: guanidinium hydrochloride (0.57 M) and formic acid (0.86%). Samples were immediately snap frozen in liquid nitrogen and stored at −80°C. Experiments were performed in triplicate.

Protein Digestion, MS/MS-Data Collection, and Peptide Identification

Samples were thawed and injected onto a UPLC system at 4°C. The protein was run over an immobilized pepsin column (Waters Corporation) at 12°C at 200 μL/min for 3 minutes, and peptides were collected on a VanGuard pre-column trap (Waters Corporation). The trap was washed for 2.5 minutes at 200 μL/min and then the peptides were eluted in-line with an Acquity 1.7 um particle, 100×1 mm C18 UPLC column (Waters Corporation), using a gradient of 10–43% B (buffer A 0.1% formic acid, buffer B 100% acetonitrile and 0.1% formic acid) over 18 minutes. Mass-spectrometry experiments were performed on a Thermo Fisher Orbitrap Elite acquiring over a mass range of 300–2000 m/z using electrospray ionization source operated at 220°C and a spray voltage of 3.8 kV. Peptides were identified using data-dependent acquisition methods following tandem-MS/MS experiments. MS/MS datasets were analysed using MaxQuant, and a false discovery rate of 1% using a database of purified proteins and known contaminants.

Mass Analysis of Peptide Centroids and Measurement of Deuterium Incorporation

To calculate the level of deuterium incorporation in each peptide, HD-Examiner Software (Sierra Analytics) was used. All peptides were manually inspected for the correct charge state, correct retention time, appropriate selection of isotopic distribution and presence of overlapping peptides. Deuteration levels were calculated using the centroid of the experimental isotope clusters. Results are presented as relative deuterium incorporation and the only control for back exchange was the level of deuterium present in the buffer. The average error of all time points and conditions was less than 0.1 Da. Cut-offs were set at 8% and 0.6 Da deuterium incorporation between conditions with an unpaired t-test value of $p < 0.05$. HDX-MS analysis statistics are presented in the Supplementary_GNE_HDX_Data as suggested by HDX-MS guidelines described by Masson et al.[24]

Conflict of Interests

The authors declare no conflict of interest.

Data Availability Statement

The data that support the findings of this study are available from the corresponding author upon reasonable request.

[1] F. G. Blix, A. Gottschalk, E. Klenk, *Nature* **1957**, *179*, 1088–1088.

[2] a) S. Kelm, R. Schauer, *Int. Rev. Cytol.* **1997**, *175*, 137–240; b) R. Schauer, *Curr. Opin. Struct. Biol.* **2009**, *19*, 507–514.

[3] a) D. Llver, P. Johansson, H. Miller-Podraza, P.-G. Nyholm, S. Teneberg, K.-A. Karlsson, in *Methods in Enzymology, Vol. 363*, Academic Press, **2003**, pp. 134–157; b) M. P. Jennings, C. J. Day, J. M. Atack, *Microbiology (Reading)* **2022**, *168*:001157.

[4] a) T. Takahashi, M. Ikegami-Kawai, R. Okuda, K. Suzuki, *Anal. Biochem.* **2003**, *322*, 257–263; b) J. E. Stencel-Baerenwald, K. Reiss, D. M. Reiter, T. Stehle, T. S. Dermody, *Nat. Rev. Microbiol.* **2014**, *12*, 739–749.

[5] S. Hinderlich, W. Weidemann, T. Yardeni, R. Horstkorte, M. Huizing, *Top. Curr. Chem.* **2015**, *366*, 97–137.

[6] A. P. Willems, L. Sun, M. A. Schulz, W. Tian, A. Ashikov, M. van Scherpenzeel, E. Hermans, H. Clausen, Z. Yang, D. J. Lefeber, *Biochim. Biophys. Acta Gen. Subj.* **2019**, *1863*, 1471–1479.

[7] R. Zeitler, A. Giannis, S. Danneschewski, E. Henk, T. Henk, C. Bauer, W. Reutter, K. Sandhoff, *Eur. J. Biochem.* **1992**, *204*, 1165–1168.

[8] P. R. Wratil, S. Rigol, B. Solecka, G. Kohla, C. Kannicht, W. Reutter, A. Giannis, L. D. Nguyen, *J. Biol. Chem.* **2014**, *289*, 32056–32063.

[9] a) F. Stolz, M. Reiner, A. Blume, W. Reutter, R. R. Schmidt, *J. Org. Chem.* **2004**, *69*, 665–679; b) S. Al-Rawi, S. Hinderlich, W. Reutter, A. Giannis, *Angew. Chem. Int. Ed.* **2004**, *43*, 4366–4370; c) A. Blume, H. Chen, W. Reutter, R. R. Schmidt, S. Hinderlich, *FEBS Lett.* **2002**, *521*, 127–132; d) J. Martinez, L. D. Nguyen, S. Hinderlich, R. Zimmer, E. Tauberger, W. Reutter, W. Saenger, H. Fan, S. Moniot, *J. Biol. Chem.* **2012**, *287*, 13656–13665.

ChemBioChem

Research Article
doi.org/10.1002/cbic.202300555

Chemistry Europe
European Chemical
Societies Publishing

[10] O. Nieto-Garcia, P. R. Wratil, L. D. Nguyen, V. Böhrsch, S. Hinderlich, W. Reutter, C. P. R. Hackenberger, *Chem. Sci.* **2016**, *7*, 3928–3933.

[11] S. Hinderlich, M. Neuenschwander, P. R. Wratil, A. Oder, M. Lisurek, L. D. Nguyen, J. P. von Kries, C. P. R. Hackenberger, *ChemBioChem* **2017**, *18*, 1279–1285.

[12] S. C. Chen, C. H. Huang, S. J. Lai, C. S. Yang, T. H. Hsiao, C. H. Lin, P. K. Fu, T. P. Ko, Y. Chen, *Sci. Rep.* **2016**, *6*, 23274–23284.

[13] S. Hinderlich, A. Sonnenschein, W. Reutter, *BioMetals* **1998**, *11*, 253–258.

[14] a) S. Hinderlich, R. Stäsche, R. Zeitler, W. Reutter, *J. Biol. Chem.* **1997**, *272*, 24313–24318; b) S. C. Chen, C. H. Huang, S. J. Lai, C. S. Yang, T. H. Hsiao, C. H. Lin, P. K. Fu, T. P. Ko, Y. Chen, *Sci. Rep.* **2016**, *6*, 23274.

[15] J.-H. Zhang, T. D. Y. Chung, K. R. Oldenburg, *J. Biomol. Screening* **1999**, *4*, 67–73.

[16] a) J. M. Bland, D. G. Altman, *The Lancet* **1986**, *327*, 908–909; b) D. Giavarina, *Biochem. Med.* **2015**, *25*, 141–151.

[17] L. A. Lor, J. Schneck, D. E. McNulty, E. Diaz, M. Brandt, S. H. Thrall, B. Schwartz, *J. Biomol. Screening* **2007**, *12*, 881–890.

[18] J. L. Gorenflos López, P. Schmieder, K. Kemnitz-Hassanin, H. C. Asikoglu, A. Celik, C. E. Stieger, D. Fiedler, S. Hinderlich, C. P. R. Hackenberger, *Chem. Sci.* **2023**, *14*, 3482–3492.

[19] D. Ghaderi, H. M. Strauss, S. Reinke, S. Cirak, W. Reutter, L. Lucka, S. Hinderlich, *J. Mol. Biol.* **2007**, *369*, 746–758.

[20] M. Liebel, J. T. Hugall, N. F. van Hulst, *Nano Lett.* **2017**, *17*, 1277–1281.

[21] T. E. Wales, J. R. Engen, *Mass Spect. Rev.* **2006**, *25*, 158–170.

[22] A. Blume, A. J. Benie, F. Stolz, R. R. Schmidt, W. Reutter, S. Hinderlich, T. Peters, *J. Biol. Chem.* **2004**, *279*, 55715–55721.

[23] M. Lisurek, B. Rupp, J. Wichard, M. Neuenschwander, J. P. von Kries, R. Frank, J. Rademann, R. Kühne, *Mol. Diversity* **2010**, *14*, 401–408.

[24] G. R. Masson, J. E. Burke, N. G. Ahn, G. S. Anand, C. Borchers, S. Brier, G. M. Bou-Assaf, J. R. Engen, S. W. Englander, J. Faber, R. Garlish, P. R. Griffin, M. L. Gross, M. Guttman, Y. Hamuro, A. J. R. Heck, D. Houde, R. E. Iacob, T. J. D. Jørgensen, I. A. Kaltashov, J. P. Klinman, L. Konermann, P. Man, L. Mayne, B. D. Pascal, D. Reichmann, M. Skehel, J. Snijder, T. S. Strutzenberg, E. S. Underbakke, C. Wagner, T. E. Wales, B. T. Walters, D. D. Weis, D. J. Wilson, P. L. Wintrode, Z. Zhang, J. Zheng, D. C. Schriemer, K. D. Rand, *Nat. Methods* **2019**, *16*, 595–602.